

where  $J$  is the exchange integral between conduction electrons and the localized spin  $S$ . The summation over lattice points on an  $xy$  plane can easily be taken, and (8) becomes

$$\rho(z) = \frac{1}{8\pi^2} \frac{2m}{\hbar^2} JS \frac{1}{2\pi} \int_{-\infty}^0 dZ \int_{-\infty}^{\infty} dq \exp[iq(z-Z)] f(q), \quad (9)$$

where we neglect the contributions from the reciprocal lattice vectors which decay exponentially with  $z$ , as far as the reciprocal lattice vectors are larger than  $2k_F$ . The integral with respect to  $q$  in (9) can be evaluated by integrating  $\exp[iq(z-Z)] f'(q)$  along the path which avoids two branch points  $q = \pm 2k_F$ , where  $f'(q)$  is the function derived by removing the symbol of absolute value from  $f(q)$ . The result is as follows:

$$\rho(z) = \frac{1}{8\pi^2} \frac{2m}{\hbar^2} JS \int_{2k_F}^{\infty} \cos(qz) \frac{4k_F^2 - q^2}{4q^2} dq. \quad (10)$$

If we put  $\alpha^2 = 2mJS/\hbar^2$ , (10) coincides with (7). For large  $z$ , (10) behaves as  $\cos(2k_F z)/(2k_F z)^2$ .

Thus, our conclusion is that in the neighborhood of the contact plane of two kinds of metals only oscillating density fluctuations are induced which originate from the Ruderman-Kittel interaction.

The authors are indebted to Professor Naga-miya who kindly suggested a simple technique for eliminating  $L$  from (4).

<sup>1</sup>J. C. Bruyere, O. Massenet, R. Montmory, and L. Néel, *Compt. Rend.* **258**, 841, 1423 (1964); O. Massenet and R. Montmory, *Compt. Rend.* **258**, 1752 (1964).

<sup>2</sup>B. Dreyfus, R. Maynard, and A. Quattropiani, *Phys. Rev. Letters* **13**, 342 (1964).

## MAGNETIC VIRTUAL LOCAL MODE CONDENSATION AND FLUORESCENCE ANOMALIES

E. W. Prohovsky

Sperry Rand Research Center, Sudbury, Massachusetts

(Received 22 December 1964)

This Letter proposes a mechanism to explain the very abrupt increase in the frequency, intensity, and lifetime of fluorescent emission, with decreasing temperature, in antiferromagnetic Mn salts. These fluorescent shifts, observed by Holloway *et al.*,<sup>1</sup> occur at a temperature  $T_H \sim \frac{1}{2}T_N$  ( $T_N$  is the Néel temperature), and are reminiscent of other fluorescent shifts which have been observed to occur at  $T_N$ .<sup>2</sup>

The experimentally observed fluorescent shifts are abrupt and suggest a cooperative transition. The absorption and emission processes in these Mn salts are a local phenomenon, however, as the excited state forms a self-trapped exciton. The concentration of excited sites is almost certainly too low for cooperative interactions to take place between the excited ions. It is proposed that a purely local effect, cooperative between local spin orientation and local lattice distortion, gives rise to these fluorescent shifts.

The proposed mechanism for altering the fluorescent emission is illustrated in Fig. 1. Curve  $a$  represents the energy of the ground state of the  $Mn^{2+}$  ion as a function of a gener-

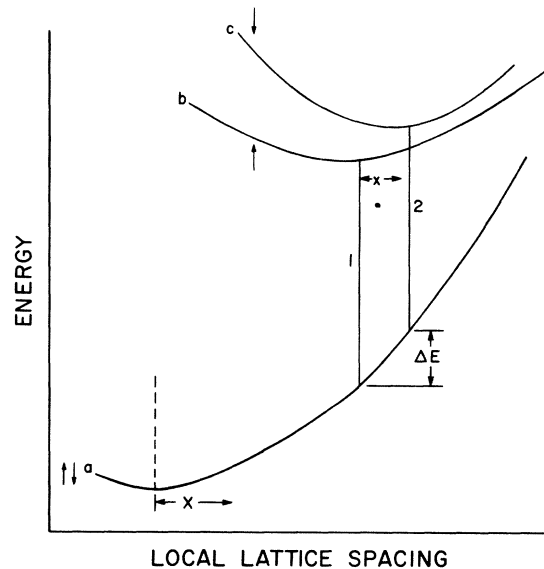


FIG. 1. A vibronic-state configuration diagram with curve  $a$  the ground state, curve  $b$  the excited state with spin aligned in the internal field, curve  $c$  the excited state with unaligned spin. Line 1 represents the emission of a photon from the aligned excited state, line 2 that from the unaligned state.

alized near-neighbor distance  $\bar{X}$ . The quadratic dependence on  $\bar{X}$  of the strain energy is the usual vibronic-state approximation.<sup>3</sup> Curve *b* represents the energy as a function of strain for the optically excited fluorescent level with the spin of the excited ion aligned in the internal magnetic field of the crystal ( $T < T_N$ ). Curve *c* is the optically excited fluorescent level with the spin of the excited ion randomly aligned in the internal field. The magnetic energy of the ion (difference between curves *b* and *c*) has been greatly exaggerated with respect to the optical splitting (difference between *a* and *b* or *c*).

More important than the actual energy difference between *b* and *c* is the fact that they have different minima in  $\bar{X}$ , i.e., there exists a magnetoelastic effect which alters the local lattice distortion about the excited ion. This distortion is then a function of the local spin orientation. The most probable neighbor configuration at the time of fluorescent emission corresponds to the minima of the excited-state curves. For aligned spins the emission follows line 1. For unaligned spins the emission follows line 2.

The energy of the fluorescent emission can be altered by  $\Delta E$  depending on the alignment of the excited-ion spin. Other properties such as lifetime, intensity, etc., can similarly be altered by changing the degree of spin alignment. The abruptness of the change in fluorescent properties comes about because the alteration in neighbor distance ( $\bar{x}$  in Fig. 1) alters the antiferromagnetic exchange energy by the magnetoelastic effect. This in turn alters the degree of spin alignment.

The magnetic alignment of an impurity or long-lived excited fluorescent ion which interacts with other sites in the crystal should be expressed in terms of the amplitude of a local magnetic mode. The ground state of the fluorescent  $Mn^{2+}$  ion has spin  $\frac{5}{2}$ , and the excited state has spin  $\frac{3}{2}$ . In addition, the exchange energy is probably reduced because one expects the interatomic spacing about the excited ion to be greater. This is due to the change in the electronic configuration of the  $Mn^{2+}$  ion from  $t_{2g}^3 e_g^2$  in the ground state to  $t_{2g}^4 e_g$  in the excited state. The excited state should then be antibonding, as pointed out by Sugano and Shulman,<sup>4</sup> which should cause local dilation.

At the position of the excited site there exists a local spin defect with lower local magnetic

energy than at other (unexcited) sites. In such a case a local mode of the virtual type exists, virtual in that its energy lies within the antiferromagnetic spin-wave quasicontinuum and interacts very strongly with the continuum spin waves. The energy of this local mode is determined by the magnetic parameters at the defect site such as the defect spin and the exchange energy between the defect and its neighbors. It is by altering the exchange energy that the local displacements ( $\bar{x}$  in Fig. 1) feed back to the magnetic system, altering the local mode and, therefore, the magnetic alignment. The direction of this cooperative effect is to reduce the energy of the virtual local mode as it becomes thermally excited. This results in further thermal excitation, etc. With decreasing temperature, on the other hand, the energy of the local mode suddenly increases as thermal de-excitation occurs, giving rise to the condensation of the local mode.

Virtual local modes in phonon spectra caused by mass defects have been investigated extensively.<sup>5,6</sup> The formation of local modes in ferromagnets has also been investigated.<sup>7</sup> One expects the results to be quite similar for antiferromagnetic spin waves. It is found that, because of the broadening by interaction with the continuum modes, a better description is to consider the virtual local mode as being made up of a superposition of continuum modes. The amplitude in the phonon case, or the alignment in the magnetic case, is primarily determined by the amplitude of a narrow band of phonons, or spin waves, with energy centered about the energy of the "would-be" local mode. The coupling of continuum modes to the defect site has been plotted in Fig. 2 of Dauber and Elliot.<sup>6</sup> The width of the virtual mode (i.e., the large number of quantum states participating in the virtual local mode) makes it possible to apply statistical averages in determining the degree of alignment of the excited ion, which greatly simplifies the analysis.

The magnetoelastic effect can be simply treated by letting

$$J^0 = J_1 + J_2(x/a), \quad (1)$$

where  $J^0$  is the total superexchange constant between the excited ion and its magnetic neighbors.  $J_1$  is the constant part,  $J_2$  is the coefficient of the linear variation with displacement, and  $x/a$  is a dimensionless displacement (see Fig. 1 for  $\bar{x}$ ). The vibrational Hamiltonian in

the vibronic-state approximation then becomes

$$H_{\text{vib}} + H_{\text{int}} = (P^2/2M) + \frac{1}{2}Kx^2 - |J_2| \tilde{S}^0 \cdot \tilde{S}^j_x/a, \quad (2)$$

where  $P$  and  $M$  are the momentum and mass associated with the vibronic state,  $K$  is its spring constant,  $\tilde{S}^0$  is the spin of the excited ion, and  $\tilde{S}^j$  is the spin at all other sites of the crystal. By completing the square in Eq. (2) one can find the new mean position of the vibronic state. This shift in mean position  $\langle x \rangle$  due to excitation of the magnetic local mode is

$$\langle x \rangle = \frac{mJ_2 \langle S_z^j \rangle}{Ka} \langle S_z^0 \rangle = \frac{mJ_2 S_z^j S^0}{KaN} [1 - \sum_{\Delta E} n(E)], \quad (3)$$

where  $m$  is the number of near neighbors,  $n(E)$  is the spin-wave occupation with energy  $E$ , and  $\Delta E$  signifies the spread over those states which make up the local mode. The sum in Eq. (3) can be limited to the states of the virtual local mode since these states provide most of the coupling to the defect site.<sup>6</sup> The average values of  $\tilde{S}^0$  and  $\tilde{S}^j$  can be taken because the sum consists of many spin-wave states even though they are all close in energy. The net thermal averages of  $\tilde{S}^j$  and  $\tilde{S}^0$  are then  $\langle S_z^j \rangle$  and  $\langle S_z^0 \rangle$ . The  $\langle S_z^j \rangle$  are the more aligned below the Néel point as they are coupled to higher energy spin waves. Since the local modes are close in energy, we will set

$$\sum_{\Delta E} n(E) = \Delta n(\bar{E}). \quad (4)$$

The defect in energy about the defect site is

$$\epsilon = (J^0 S^0 - J^j S^j) S^j. \quad (5)$$

When this parameter is negative the modes are virtual. Making use of Eqs. (1), (4), and (5), this becomes

$$\epsilon = -|\epsilon_0| - |\epsilon_1| n(\bar{E}). \quad (6)$$

The energy  $\bar{E}$  of the local mode should decrease monotonically with decreasing  $\epsilon$ . This is shown by Dauber and Elliot<sup>6</sup> to be the case for phonons. To a first approximation we will assume

$$\bar{E}(T) = E_0' + \beta\epsilon, \quad (7)$$

and using Eq. (6),

$$\bar{E}(T) = E_0 - \alpha n(\bar{E}). \quad (8)$$

The linear approximation [Eq. (7)] holds in

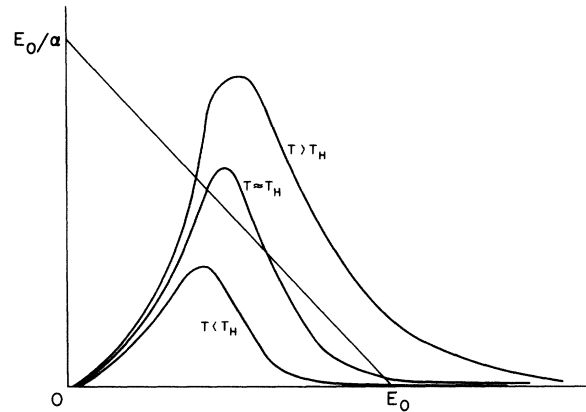


FIG. 2. The solution  $\bar{E}$  of Eq. (7) is given by the intersection of the line  $(E_0 - \bar{E})/\alpha$  with  $n(\bar{E}) = \bar{E}^2 (e^{\bar{E}/KT} - 1)^{-1}$ . For  $T < T_H$ , the solution is very close to  $E_0$ . For  $T > T_H$ , the solution is very much less than  $E_0$ . The change is discontinuous with some possibility of unstable solutions at  $T \approx T_H$ .

the phonon case for large negative  $\epsilon$ .<sup>5</sup> Equation (8) shows cooperative behavior, giving rise to discontinuous changes in the solution for  $\bar{E}$ . The solutions are illustrated in Fig. 2. There is a striking formal similarity between Eq. (8) and that derived by Adler and Feinleib<sup>8</sup> for describing semiconductor-to-metal transitions. As  $\alpha$  approaches zero, however, the change in energy of the local mode at the transition also vanishes. Even when the assumption of linearity [Eq. (7)] does not hold exactly, transitions would, in general, still be expected as the line  $(E_0 - \bar{E})/\alpha$  could contain curvature and still give rise to discontinuous solutions for  $\bar{E}$ . An evaluation of the magnitude of  $\alpha$ , as well as the actual dependence of  $\bar{E}$  on  $\epsilon$ , awaits the application of local-mode theory to antiferromagnetism.

The author wishes to thank Dr. W. W. Holloway, Jr., Dr. M. Klein, Dr. J. Shane, and Professor H. Ehrenreich for many helpful discussions.

<sup>1</sup>W. W. Holloway, Jr., M. Kestigian, R. Newman, and E. W. Prohofsky, Phys. Rev. Letters **11**, 82 (1963).

<sup>2</sup>W. W. Holloway, Jr., and M. Kestigian, Phys. Rev. Letters **13**, 235 (1964).

<sup>3</sup>C. C. Klick and J. J. Shulman, Phys. Rev. **42**, 910 (1952).

<sup>4</sup>S. Sugano and R. G. Shulman, Phys. Rev. **130**, 517 (1963).

<sup>5</sup>R. Brout and W. Visscher, Phys. Rev. Letters **9**, 54 (1962).

<sup>6</sup>P. G. Dauber and R. J. Elliot, Proc. Roy. Soc. (London) **A273**, 222 (1963).

<sup>7</sup>T. Wolfram and J. Callaway, Phys. Rev. **130**, 2207

(1963).

<sup>8</sup>D. Adler and J. Feinleib, Phys. Rev. Letters **12**, 700 (1964).

### DEPENDENCE OF THE SUPERCONDUCTING TRANSITION TEMPERATURE ON CARRIER CONCENTRATION IN SEMICONDUCTING SrTiO<sub>3</sub>†

J. F. Schooley, W. R. Hosler, E. Ambler, and J. H. Becker\*  
National Bureau of Standards, Washington, D. C.

and

Marvin L. Cohen‡ and C. S. Koonce  
Department of Physics, University of California, Berkeley, California  
(Received 21 January 1965)

The superconducting transition temperature of reduced SrTiO<sub>3</sub><sup>1</sup> has been measured as a function of electronic carrier concentration,  $n_c$ , over three orders of magnitude, i.e., from  $10^{18}$  to  $10^{21}$  carriers/cm<sup>3</sup>. The transition temperature exhibits a maximum in the range of carrier concentration investigated. The dependence of the transition temperature on carrier concentration can be understood on the basis of the assumption that the superconductivity arises primarily from the attractive interaction resulting from the exchange of intervalley phonons between time-reversed electron pairs, and reveals interesting screening effects arising from the free carriers.

The superconductive transitions were observed by measuring the magnetic susceptibility using an ac method at 210 Hz and 0.01-Oe measuring field, and also by four-lead resistance measurements. External fields were compensated to about 0.01 Oe.

The specimens were prepared by appropriate reduction of single crystals of SrTiO<sub>3</sub>.<sup>1</sup> The carrier concentrations were determined from Hall-effect measurements at 300, 77, and 4°K.<sup>2</sup> As noted in reference 1, representative specimens were measured by x-ray diffractometer techniques to detect possible second-phase contamination, particularly Ti and TiO. To the limit of sensitivity of the technique (about ½%), specimens over the whole range of carrier concentration were shown to be single crystals of SrTiO<sub>3</sub> perovskite structure. The electrical-resistance specimens were thin slabs approximately 10×3×1 mm, and the magnetic susceptibility specimens were rough spheres of 3 mm diameter.

The specimens were cooled to temperatures as low as 0.05°K through thermal contact with

a few hundred copper wires imbedded in a chromium-potassium-alum pill which was cooled by adiabatic demagnetization. The specimen temperatures were deduced from the paramagnetic susceptibility of a separate chromium-potassium-alum single-crystal sphere 3 mm in diameter which was also in thermal contact with the copper cooling wires at a position beyond the specimens. In order to reduce the time required for each run, the chrome-alum pill was electrically heated between measurements.

Typical examples of the transitions as observed magnetically and resistively are shown in Fig. 1. The electrical specimens generally first showed resistance at a temperature very nearly that of the upper end of the corresponding transition observed magnetically. The transitions are rather broad in tempera-

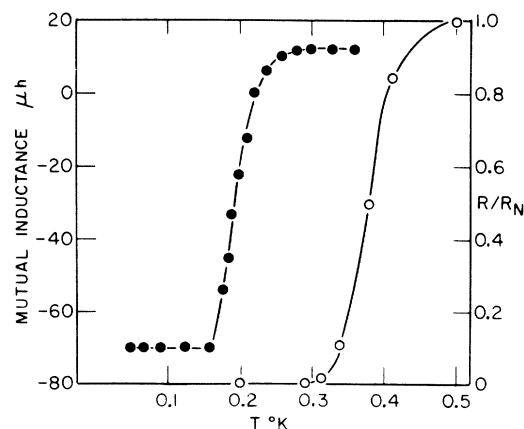


FIG. 1. Superconductive transitions at  $n_c = 2.5 \times 10^{19}$  cm<sup>-3</sup>. The left-hand ordinate (filled circles) reflects the magnetic specimen susceptibility, and the right-hand ordinate (open circles) shows the ratio of electrical specimen resistance to the normal value, which is constant up through the helium range.